Two-dimensional transition metal chalcogenide crystals modified by individual hetero-atoms

- final report -

The main goal of the present project was engineering the atomic structure of 2D materials, in order to tune their properties for desired functionalities, such as enhancing their catalytic activity, modifying their electronic or optical properties. According to the plan, the investigated materials mainly come from the family of transition metal chalcogenides, while the primary engineering strategy was proposed to be the incorporation of heteroatoms into the structure of 2D crystals. The original hypothesis was that O atoms incorporated into the crystal lattice of 2D transition metal chalcogenides (as realized by us earlier) can be replaced by other heteroatoms, such as Pt, Au or Fe, activating the further enhancement of the catalytic activity of the basal plane of various 2D crystals, as well as tuning their electronic and optical properties. Our original approach for the incorporation of heteroatoms was their electrochemical deposition. However, it turned out that the incorporation of a single metal heteroatoms into the structure of 2D crystals is rather challenging, in spite of the availability of surface vacancy sites, which can act as anchor sites for heteroatoms. Nevertheless, our efforts to incorporate individual heteroatoms into 2D crystals resulted in a series of interesting results, even surpassing our original expectations regarding their effect on the catalytic performance. While various 2D crystals have been investigated, for metal decoration and catalytic applications, 2D MoS_2 crystals turned out to be the most suitable. As concerning various heteroatoms, within this project, the best results have been achieved with platinum (Pt), gold (Au), and iron (Fe). Using electrochemical deposition, we were able to deposit on 2D MoS_2 crystal, ultra-fine Pt clusters of less than 20 atoms, and Au clusters consisting of a few tens of atoms. More importantly such ultra-small Pt and Au clusters acquired a novel atomic structures, namely bilayer Pt and monolayer Au structures. Such structures are not stable in free-standing form, but are stabilized by their strong interaction with 2D MoS_2 crystals. We were able to reveal the electronic structure (local density of states - LDOS) of these quasi-2D metal clusters by tunneling spectroscopy investigations. In both cases, a nonmetallic electronic structure has been observed with a 03 - 0.4 eV energy gap observed in Pt bilayers, and 0.5 - 1 eV energy gap measured in monolayer Au clusters. In contrast to Pt, which is the best catalyst for hydrogen production, bulk gold is mostly inert. However, our nonmetallic monolayer Au clusters displayed a strongly enhanced catalytic activity, substantially improving the catalytic properties of 2D MoS_2 crystals in catalyzing the hydrogen evolution reaction. Through the realization of ultra-fine bilayer Pt clusters, characterized by a sizeable energy gap in their electronic structure, we were able to investigate, for the first time, the catalytic properties of nonmetallic Pt nanoparticles. Remarkably, we found that nonmetallic Pt bilayers display a drastically increased catalytic activity for hydrogen evolution, compared to conventional metallic Pt nanoparticles. Our nonmetallic Pt bilayers produce hydrogen at ten times higher rates than the best Pt catalysts reported before.

Since the electrochemical decoration of 2D crystals with individual metal heteroatoms proved to be more challenging than expected (instead, highly active small clusters can be deposited with high efficiency), we have continued to explore alternative approaches. We have successfully developed a novel route for anchoring single Fe atoms on the surface of 2D MoS_2 crystals, through the immobilization of an iron complex (Fe(tia-BAI)Cl_2), comprising a single Fe atom. A substantially improved catalytic activity for hydrogen evolution was observed on 2D MoS_2 crystals decorated by individual Fe atoms, compared to pristine 2D MoS_2 crystals.

Besides the main focus of the project on 2D transition metal chalcogenide crystals and heteroatom (cluster) modifications, novel directions also emerged while implementing the project. Besides heteroatom incorporation, mechanical strain is also known to be highly efficient in engineering the catalytic, electronic and optical properties of 2D materials.

We have investigated the effect of strain on a novel van der Waals material: $ZrTe_5$. To study the effect of strain experimentally, we have performed tunneling spectroscopy measurements on $ZrTe_5$ nanobubbles that are characterized by complex strain fields. We found that mechanical strain enables the tuning of the electronic structure between a strong and a weak topological insulator phase, which transition occurs through a metallic state. We also found that mechanical deformation can close the band gap in $ZrTe_5$ monolayers, while $ZrTe_5$ bilayers exhibits both topological insulating, trivial metallic and insulating phases. We have found by scanning tunneling microscopy investigations that while $ZrTe_5$ monolayers are difficult to exfoliate without compromising their crystalline structure, but $ZrTe_5$ bilayers offer a stable alternative for experimental studies of topological phase transformations.

We have also developed a novel nanoengineering technique that enables us to induce unprecedentedly strong nanoscale structural deformations into the atomic structure of graphene. We found that such deformations can induce a localization of charge carriers, and most importantly, they can efficiently confine graphene plasmons into sub-5nm areas, scaling up their plasmon resonance frequency from native THz values into the commercially relevant visible-frequency range. This way, we have realized for the first time visible-frequency graphene plasmons, and were able to directly detect them by scanning near-field optical microscopy (SNOM) investigations. As a first application, we have demonstrated a strong enhancement of the Raman signal of molecules in the vicinity of the nanocorrugated graphene sheets, enabling the detection of specific molecules even from femtomolar solutions, demonstrating a three orders of magnitude lower detection limit than previously achieved with graphene based optical sensors.

2D MoS_2 crystals can stabilize semiconducting Pt structures

Decreasing the size of the metal nanoparticles is a viable route to reduce noble metal utilization efficiency in catalysts. As the metal particle size is reduced, besides increasing the fraction of accessible surface atoms, an energy gap is also expected to open, below a critical size, due to quantum confinement effects. However, experimentally realizing and studying an energy gap in metal nanoparticles, turned out highly challenging. An energy gap has been observed in small Au nanocrystals, particularly, when their thickness has been reduced to one or two atomic layers. The observation of an energy gap in Pt nanostructures turned out even

more challenging, hence the catalytic properties of nonmetallic Pt nanocrystals remained largely unexplored. We emphasize that here we focus on unoxidized, elemental Pt nanoparticles, as opposed to oxidized Pt structures that have been studied before, and are often also referred to as nonmetallic Pt.

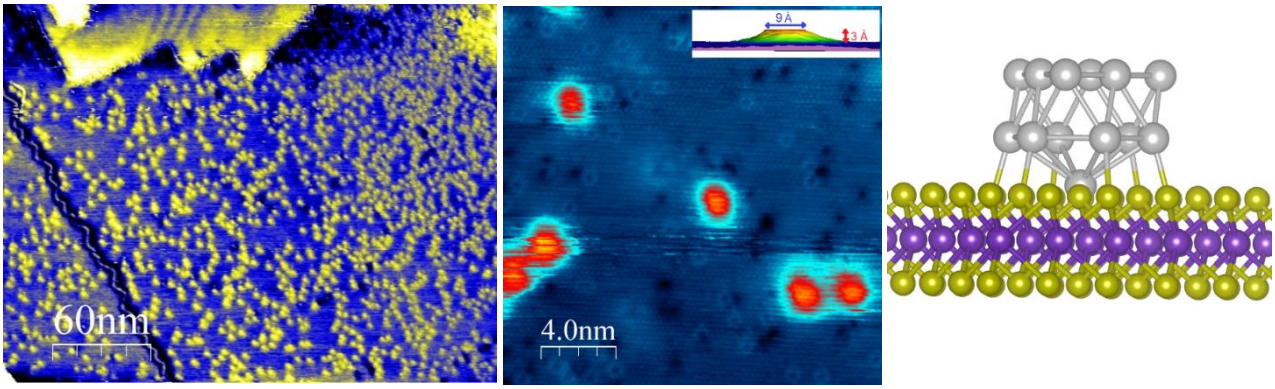

Fig.1. *STM image of Pt nanoclusters of about 1nm diameter and 0.3nm height, electrochemically deposited on 2D MoS_2 crystals. The flattened geometry corresponding to two Pt atom thickness, indicates a strong metal-support interaction. The smaller bright and dark features in the STM image correspond to S atom vacancy defects of the 2D MoS_2 support that can act as anchors for stabilizing ultra-fine Pt clusters. b) Simulated (DFT) structure of a Pt_{13} cluster anchored to a S atom vacancy of the 2D MoS_2 crystal, reproducing the experimentally observed bilayer Pt structure.*

Metal-support interaction is a powerful tool for engineering the atomic and electronic structure of metal nanoparticles. While MoS_2 is regarded as a rather weakly interacting support, the chemical affinity between Pt and S holds the potential for a strong interaction.

However, unleashing the full strength of Pt-MoS_2 interactions for Pt nanocrystals is hindered by their large (> 10%) lattice mismatch with MoS_2. A better interface matching can be achieved for small (< 1 nm) Pt clusters, due to their higher plasticity. However, we show that under proper kinetic deposition conditions, a strongly enhanced adhesion can be realized between small (~1nm) Pt clusters and 2D MoS_2 crystals.

Gaining information on the electronic structure of Pt nanoparticles is of key importance for understanding and optimizing their catalytic performance. This, is of particular importance in our case, since both the flattened morphology (quantum size effects), and the enhanced metal-support interaction are expected to have a strong influence on the electronic structure. While tunneling spectroscopy measurements can directly probe the electronic structure of metal nanostructures, the available data on catalyst nanoparticles is very scarce. This is mainly due to charging effects, owing to the weak electronic coupling to the support. Due to the enhanced coupling emerging from the stronger Pt/MoS_2 interaction, we were able to resolve the fine details of the local density of states (LDOS) of small Pt clusters by tunneling spectroscopy, within the energy window (-1.8 eV to + 0.3 eV), opened by the band gap of the 2D MoS_2 support. The most striking feature, is a sizeable energy gap of about 0.3 eV, with fully supressed Pt LDOS near the Fermi energy (0 V), evidencing the nonmetallic nature of bilayer Pt clusters (Fig.2a).

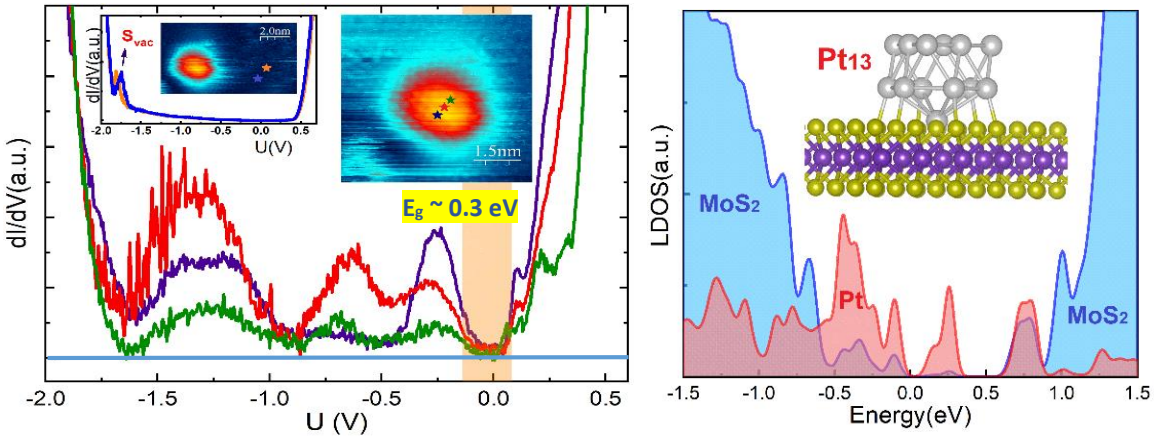

Fig. 2. *a) Tunneling spectra recorded on a Pt cluster at the positions marked in the right inset, revealing a bandgap of ~300 meV. Left inset shows the tunneling spectra on MoS_2 away from Pt clusters, with a single peak characteristic to sulphur vacancies. b) Calculated (DFT) local density of states (LDOS) of a Pt_{13} cluster, anchored by an S_{vac} to the 2D MoS_2 support. Red and blue areas represent contributions from the Pt cluster and the MoS_2 support, respectively.*

To compare with the measured STM data, we have calculated the topographic STM images of the simulated bilayer Pt cluster structures, and found their heights to be about 3-4 Å, in good quantitative agreement with the experimentally measured cluster heights. To directly compare with our tunneling spectroscopy measurements, we have calculated by DFT the local density of states (LDOS) of such bilayer Pt clusters adsorbed on 2D MoS_2, comprising 10, 13 and 27 Pt atoms. We found that all the investigated bilayer Pt clusters are characterized by a sizeable energy gap at the Fermi level, in good agreement with the experimental findings. The calculated LDOS of the Pt_{13} clusters (Fig. 2b) displays the best agreement with tunneling spectroscopy measurements (Fig. 2a), which also matches the size of the measured clusters most closely.

The large-scale and environmentally friendly production of hydrogen, requires highly active, stable and cost-efficient catalysts. While platinum is known as the most efficient catalyst for hydrogen evolution, its high costs and scarcity strongly limit its practical use in large-scale applications. To overcome this, extensive efforts have been focused on replacing platinum with cheaper, more abundant materials, as well as on reducing the Pt content of catalysts, while maintaining the outstanding activity and stability. Among the most successful approaches are those based on improving Pt atom utilization efficiency through improving dispersion, which is maximized in Pt single atom catalysts (SACs). Indeed, such catalysts were able to reach the activity of commercial Pt/C catalysts, with two orders of magnitude lower Pt loadings of order of microgram/cm^2. However, SACs represent the end of the road in terms of catalyst design for approaches relying on dispersion. To further reduce the Pt loading, without losing activity, one needs to design Pt structures that outperform the intrinsic activity of conventional Pt nanoparticles and Pt SACs.

Distorted Pt structures are known to host reaction sites of increased intrinsic activity. However, this comes at the price of a substantially reduced stability. Therefore, engineering novel Pt structures is a compromise between increasing activity and preserving stability. We have observed that the catalytic performance of the Pt/MoS_2 system can be substantially improved by realizing small Pt clusters that interact more strongly with the MoS_2 support.

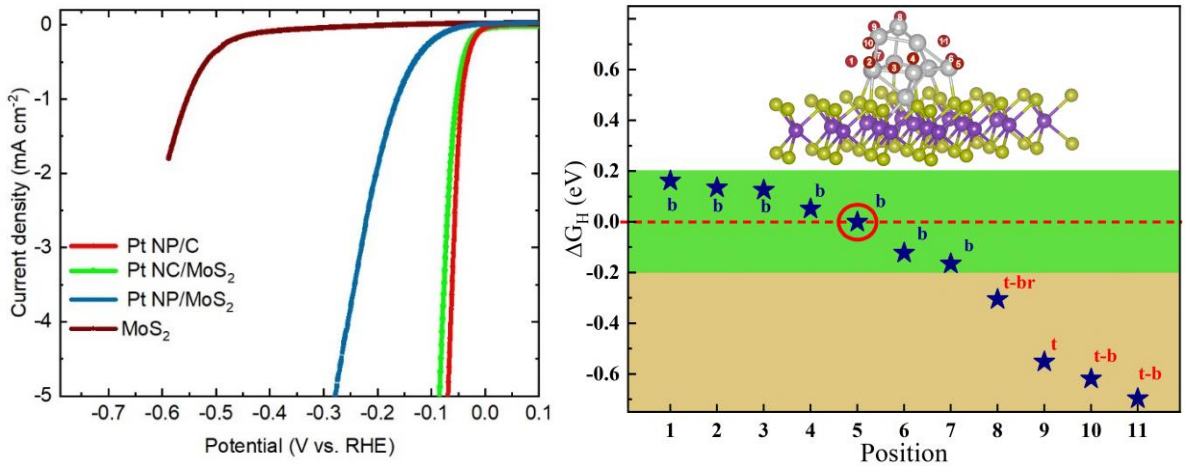

Fig. 3. *Linear sweep voltammetry measurements on various samples revealing that the Pt nanoclusters on MoS_2 can closely approach the activity of commercial Pt-C catalysts at orders of magnitude lower Pt content (left). Theoretical model of Pt nanoclusters on MoS_2 and the corresponding H adsorption free energies, indicating the presence of highly active sites at the Pt/MoS_2 interface-perimeter sites.*

2D MoS_2 crystals decorated with small Pt clusters display exceptionally high catalytic activity towards hydrogen evolution. Such ultra-fine clusters perform much better than larger (~5 nm) Pt nanoparticles deposited on MoS_2, even though the Pt content is three orders of magnitude lower for samples comprising small Pt clusters (Fig.3a). Most importantly small Pt clusters on MoS_2 samples closely approach the activity of commercial Pt-C catalysts, again at three orders of magnitude lower Pt content. We attribute the observed outstanding efficiency of our catalyst to a strongly increased Pt/MoS_2 interaction, leading to: (1) the stabilization of ultra-fine Pt clusters all over the MoS_2 basal plane, (2) deformation of Pt clusters morphology into a quasi-flat (bilayer) structure, in order to take better advantage of Pt-S interactions, and (3) a spectacular increase of the intrinsic activity of Pt sites, allowing orders of magnitude reduction of Pt loading, compared to commercial Pt/C catalysts, without losing activity or stability. Detailed simulations of hydrogen adsorption free energies revealed that the most active sites are on the Pt atoms directly adhering to the MoS_2 surface (Fig. 3b), indicating strong synergistic effects at the origin of the outstanding catalytic performance.

Single atom thin Au nanocrystals on 2DMoS_2 for enhanced catalytic activity

In contrast to Pt, which is known to be the best catalyst for hydrogen evolution, gold (Au) is rather inert in catalyzing this reaction. However, we have found that a novel gold structure of a single atom thickness (and 2-5 nm lateral size) can be stabilized on the surface of 2D MoS_2 crystals, substantially enhancing the catalytic activity of MoS_2, towards hydrogen evolution. The Au decorated MoS_2 samples have been investigated by high resolution transmission electron microscopy measurements. In order to achieve this, a novel sample preparation method has been developed, peeling of the top few layers of the bulk graphite crystal, supporting the 2D MoS_2 crystal that in turn are decorated by the small Au clusters. TEM investigations reveled a dense decoration of the MoS_2 crystals with Au nanoclusters of a few nm diameters. The height of the Au clusters cannot be directly measures in TEM, however,

they must be relatively thin as these Au clusters did not show up in the scanning electron microscopy images.

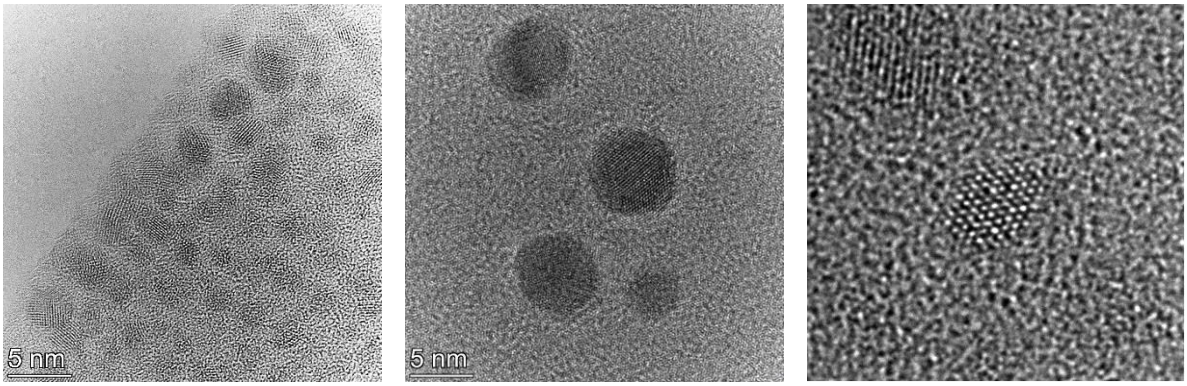

Fig. 4. *High resolution transmission electron microscopy revealing Au clusters of a few nanometer lateral size. Atomic resolution is achieved on Au clusters, however, their interpretation is not straightforward, as the resulting patterns originate from the superposition of three different crystal structures: graphite, MoS_2, and Au.*

We have employed scanning tunneling microscopy investigations to reveal the thickness of the Au nanoclusters deposited on 2D MoS_2 crystals by electrodeposition.

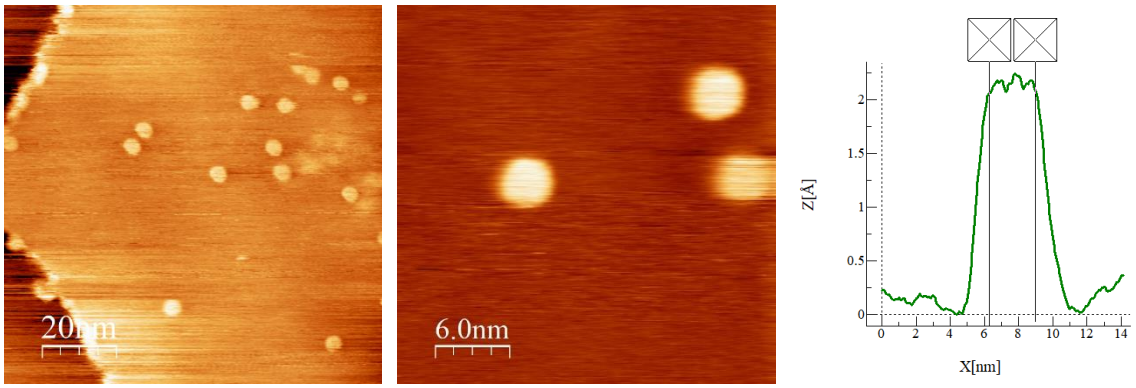

Fig. 5. *Scanning tunneling microscopy investigation of Au nanoclusters deposited on 2D MoS_2 crystals, revealing a flat morphology of the Au clusters with their thickness less than 0.2 nm, corresponding a monolayer of Au atoms. The lateral size of Au nanoclusters is of a few nanometers, in accordance with the TEM measurements.*

Our STM investigation revealed the presence of Au nanoclusters with a few nanometers lateral size and a thickness of less than 2 A. This, most likely corresponds to a single layer of gold, stabilizing a 2D crystal form of gold on 2D MoS_2 crystals.

We have also performed tunneling spectroscopy measurements on such 2D Au nanoclusters, revealing a large energy gap of about 0.8 eV (Fig.6). Unlike for Pt, the opening of an energy gap has been reported previously in gold nanoclusters, when their thickness is reduced to a one or two layers of gold atoms.

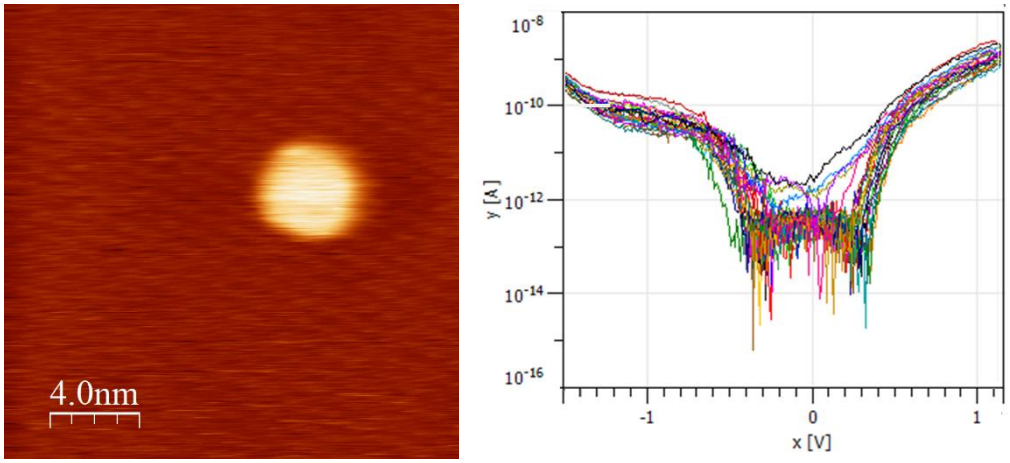

Fig. 6. *Scanning tunneling microscopy image of an Au nanoclusters on 2D MoS_2 with the corresponding tunneling spectra, revealing a fully suppressed local density of electronic states near the Fermi level (0V), of a width of about 800 meV.*

2D gold nanocrystals stabilized on 2D MoS_2 were found to be characterized by a nonmetallic electronic structure with energy gaps in the range of 0.5 - 1 eV.

We have investigated the catalytic properties of these nonmetallic Au monolayers, by performing linear sweep voltammetry. The corresponding results are shown in Fig. 7.

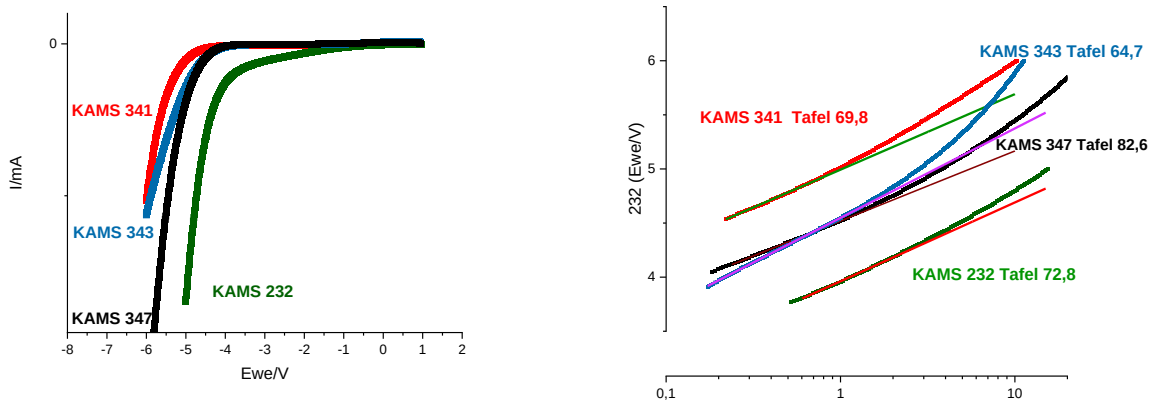

Fig.7. *Linear sweep voltammetry measurements on various samples revealing that nonmetallic 2D gold nanoclusters (KAMS 232) improve the most the activity of 2D MoS_2, and are more active than other gold nanoparticles, in spite of comprising orders of magnitude lower amount of gold.*

As a control experiment we have grown these 2D gold clusters into larger Au nanoparticles with conventional 3D structures. Such samples displayed a decreased catalytic activity, in spite of adding more gold to the system. This emphasizes the key role of the novel 2D gold structure and their nonmetallic electronic structure in enhancing the catalytic activity. Furthermore, our Scanning Tunneling Microscopy investigations revealed that ultra-fine gold nanoclusters also decorate the edges of 2D MoS_2 crystals, which are known to be the inherently active sites of MoS_2. We found that decoration of MoS_2 edges by ultra-fine gold clusters further enhances their catalytic activity. A manuscript comprising the results on 2D Au clusters decorated MoS_2 crystals is under preparation, and will be published with the present OTKA project as funding source.

2D MoS_2 crystals decorated with individual Fe atoms

The properties of 2D transition metal chalcogenides can be also fine-tuned by chemical modifications strategies, however, these materials are rather inert, that make things difficult when it comes to chemical derivatization. The application of first-row transition metal coordination complexes as molecular catalysts in hydrogen evolution reaction (HER) is another promising path towards cheap and efficient hydrogen production. In order to take benefit from the catalytic opportunities of both approaches, we have developed a simple and convenient method to immobilize Fe(tia-BAI)Cl_2 (tia-BAI¯=1,3-bis(2'-thiazolylimino)isoindolinate(¯)) on the surface of MoS_2 nanosheets. FeIII(tia-BAI)Cl_2 a five-coordinate, distorted trigonal bipyramidal structure complex with the tridentate, anionic tia-BAI−ligand occupying the two apical and one equatorial positions in a meridional topology (Fig.8). The two thiazole-based coordinative Fe-N bonds are of equal length (2.095 Å), while the bond between the pyrollic nitrogen atom and the iron centre is somewhat lower (2.019 Å), indicating a stronger interaction. The possibility of the coordination of solvent molecules to the iron(III) central atom, highlighted the opportunity to immobilize the complex on the surface of MoS_2, through the formation of coordinative Fe-S bonds. Soaking MoS_2/HOPG samples in the methanol solution of Fe(tia-BAI)Cl_2 lead to the formation of Fe(tia-BAI)-MoS_2/HOPG hybrid nanomaterials. As a result of the surface modification, three new peaks appeared in the Raman spectrum of Fe(tia-BAI)-MoS_2/HOPG, in addition to the peaks related to MoS_2 (381 and 410 cm^{-1}) and to HOPG (1583 cm^{-1}). The new peaks at 1364, 1412 and 1614 cm^{-1} can be assigned with most intensive peaks of the complex, presumably related to the C=C and C=N stretching vibration modes.

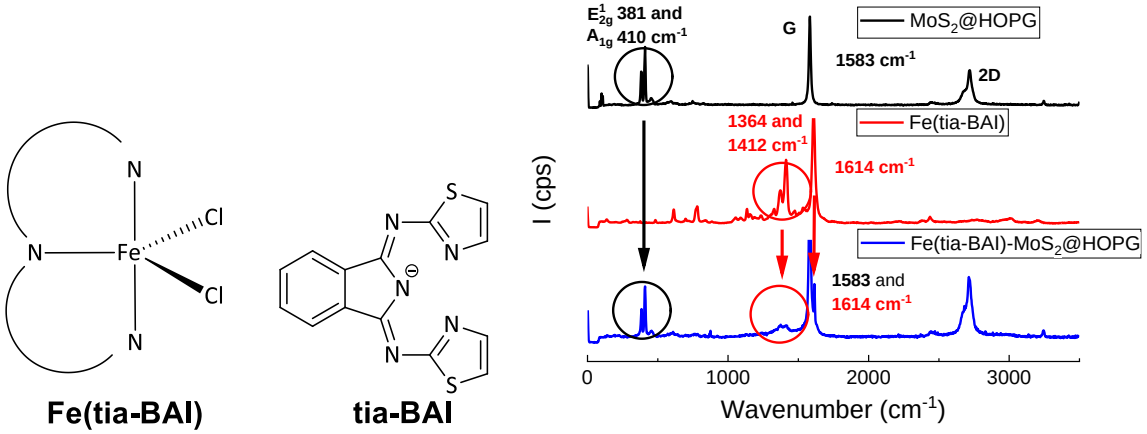

Fig 8. *Structure of FeIII(tia-BAI)Cl_2 and Raman spectra corresponding to the bare MoS_2/HOPG (top), Fe(tia-BAI)Cl_2 and Fe(tia-BAI)-MoS_2/HOPG*

The presence of iron complex on the surface is clearly indicated by the similarity of the infrared spectrum of Fe(tia-BAI)Cl_2 and the spectrum of the modified MoS_2 samples. The C=C stretching vibration peak can be identified in the IR spectrum of Fe(tia-BAI)Cl_2 at 1607 cm^{-1}, as well as in the spectrum of Fe(tia-BAI)-MoS_2.

We have further investigated our Fe(tia-BAI) functionalized MoS_2 samples, by STM measurements, revealing the presence of single molecules stably anchored on the surface of MoS_2, as even room temperature STM measurements could not sweep them away (Fig. 9).

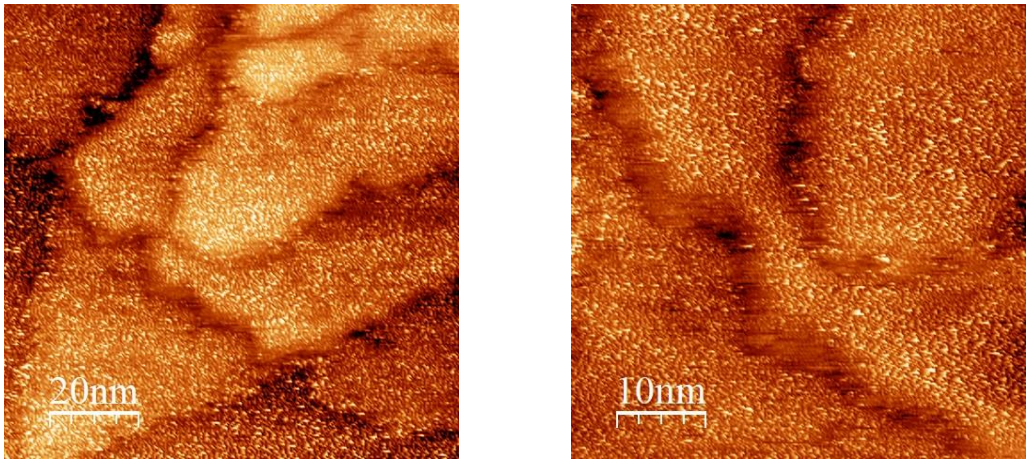

***Fig.9**. STM image of 2D MoS_2 single and few layer crystals decorated by Fe(tia-BAI) molecules comprising a single Fe atom. Such molecules of about 1 nm diameter appear as bright dots in the STM image.*

Therefore, we were able to confirm the immobilization of the iron complex on the surface of 2D MoS_2 crystals by directly imaging them with Scanning Tunneling Microscopy.

In order to investigate, how the presence of the iron complex on the surface can influence the catalytic properties of MoS_2 nanostructures in hydrogen evolution, polarization curves were obtained on the same sample before and after functionalization.

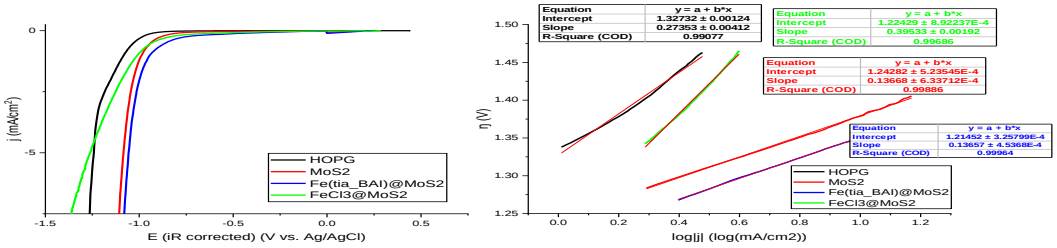

***Fig. 10** Linear sweep voltammetry measurements and the corresponding Tafel slopes of various samples revealing that 2D MoS_2 crystals fuctionalized by individual Fe atoms display a clearly increased activity for the hydrogen evolution reaction.*

Measurements were also performed on an unmodified graphite crystals as reference. The linear voltammograms and the corresponding Tafel plots (Fig. 10) revealed an increased catalytic activity of the functionalized sample, compared to bare MoS_2. Another MoS_2 sample was drop casted with $FeCl_3$ solution and polarization curve under the same experimental conditions was obtained to examine if the enhanced catalytic activity on MoS_2 could be also achieved by other iron compounds. Although $FeCl_3$@MoS_2 sample showed a slight current increase, compared to HOPG, its activity was far behind Fe(tia-BAI)@MoS_2 and the high Tafel constant of 395.3 mV/dec, obtained, also suggested a sluggish kinetics for hydrogen evolution.

In conclusion, we could achieve a substantially improved catalytic activity for hydrogen evolution with 2D MoS_2 crystals decorated by individual Fe atoms. A manuscript comprising the results regarding the preparation and catalytic activity of Fe(tia-BAI)Cl_2 is under the second review round in Dalton Transactions, while the manuscript comprising the results on singe Fe atom decorated MoS_2 crystals is under preparation, it will be submitted for publication during the next months with the present OTKA project as the funding source.

Strain engineering the electronic structure of $ZrTe_5$

Three-dimensional time reversal symmetric topological band insulators are classified into "strong" (STI) and "weak" (WTI) according to the nature of their surface states. The surface states of the STI are topologically protected from localization, while this does not hold for the WTI. These phases are generally separated by a metallic, conducting Dirac or Weyl semimetal phase. To change the indices, it is necessary to close and reopen the bandgap through of the metallic phase. Among the transition-metal pentatellurides, $ZrTe_5$ is an excellent material to investigate the topological phase transitions. This material has been widely studied because it has numerous exotic and therefore interesting physical properties. The topological nature of the bulk $ZrTe_5$ has not been unambiguously identified so far. Here, we have investigated the characteristics of the crystal using state-of-the-art experimental STM techniques and computer modeling on a multilayer $ZrTe_5$ bubble, formed by the contamination trapped between the $ZrTe_5$ crystal and the substrate. The unique strain pattern of the bubble allowed tuning of the originally strong topological insulating phase of the crystal into a metallic phase at the perimeter of the bubble. This transition can be observed using tunneling spectroscopy measurements (Fig 11.b). The halo of the bubble of this highly anisotropic material is only present at two sides of the bubble, where the crystallographic orientation matches the Te-Te chains direction. In the perpendicular direction there is no observable phase transition.

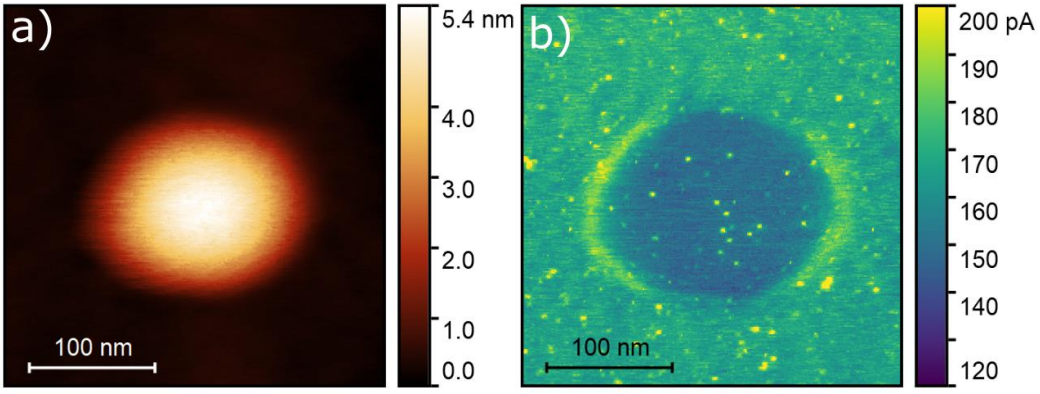

***Fig. 11**. a) STM topography image of a $ZrTe_5$ bubble. b) Tunneling spectroscopy mapping of the same area. The perimeter of the bubble displays high density of states segments, indicating a metallic phase in certain directions.*

To understand the experimentally observed behavior, we first must establish a proper description of the elasticity tensor of the material. For this reason, we determined the elasticity tensor elements using density functional theory (DFT) calculations, as the free energy obtained from DFT of a mechanically distorted crystal is a function of the strain pattern of the distortion.

This way we were able to obtain the full elasticity tensor of the material. Then, by numerically solving the three-dimensional equation of motion by the finite element method (FEM), implemented in the COMSOL package, we were able to determine the strain pattern of the bubble. This procedure has allowed us to explain the observed features without the necessity of any phenomenological models or fitting parameters.

We obtained the electronic properties by DFT of a distorted crystal using the strain pattern that we determined from the FEM method at the two semi-axes of the bubble. Along the major semi-axes DFT predicts that the band gap is closed, hence the density of states increases. On the contrary, in the vicinity of the minor semi-axes the *ab initio* analysis shows a small topologically strong band gap, therefore the density of states remains low. These *ab initio* results are in excellent agreement with our measurements.

By establishing the equilibrium state of the crystal, we can map the topological phase diagram of the crystal using *ab intio* methods. Fig. 12 shows the contour map (phase diagram) of the size of the bandgap under various mechanical strains. The horizontal (vertical) axes indicate the strain along the in-plane (out-of-plane) lattice directions obtained by DFT. At every point a sign has been assigned to the gap as the topological invariants were calculated. Positive (negative) sign indicates weak topological (strong topological) insulating phase. The phase diagram shows three main domains. Around the equilibrium the system is a STI (1). However, by applying mechanical strain, it can be tuned to the WTI phase (3). Between the two insulating phases there is a conducting phase (2). The black line in the conducting phase shows where the Dirac cones in the gamma point touch each other.

The results were also tested using a fundamentally different DFT code and the outcome was found to be in excellent agreement with our previous results. Our results not only clarify the controversies regarding the strong/weak TI nature of $ZrTe_5$, but also provide the full, experimentally tested elasticity tensor of the material.

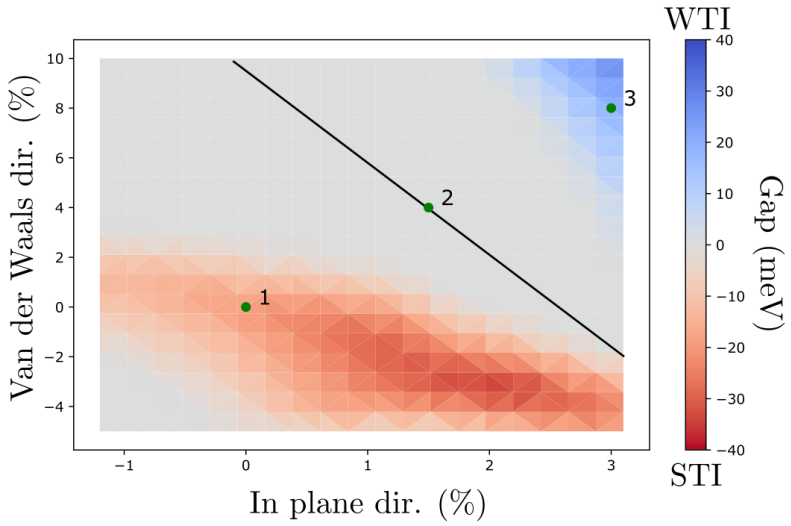

Fig. 12*. The phase diagram of the electronic structure of the crystal under mechanical strain. The three main domains are marked by numbers. (1) is strong TI, (2) is metallic and (3) is the weak TI phase. The black tentative line indicates where the Dirac cones touch each other.*

Since $ZrTe_5$ lies at the boundary of the weak and strong topological phases, making tuning by mechanical strain a viable strategy to realize transitions between topological phases. This material is particularly interesting also due to its numerous exotic properties, such as the planar Hall effect, anomalous Hall effect and chiral magnetic effect. However, most studies have focused on the bulk material, with very few experimental results on monolayers, even though in the single layer the crystal is predicted to be a large gap 2D topological insulator.

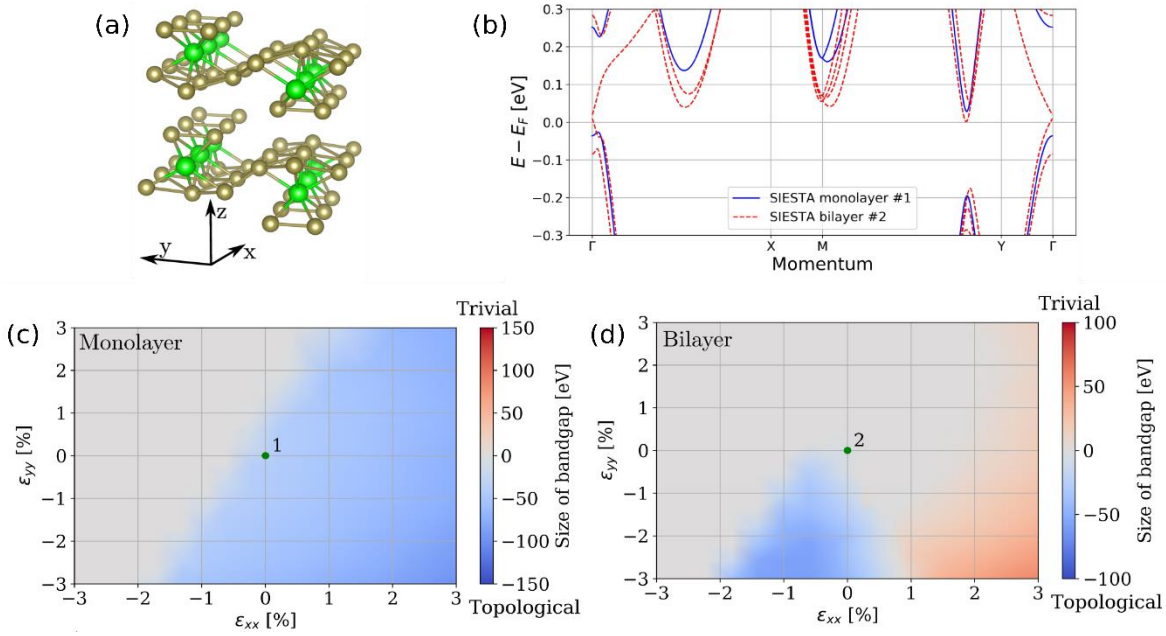

Fig. 13. *Topological phases of mono and bilayer $ZrTe_5$. (a) Crystal structure of ZrTe5, showing two van der Waals monolayers, extending along the x, y plane. (b) Band structure of the monolayer and bilayer. Density plot of the band gap for the monolayer (c) and bilayer (d). Red and blue colors represent the topological character of the gap (see also ref.* ***Hiba! A könyvjelző nem létezik.****) as a function of biaxial in plane (ε_{xx}) and out of plane (ε_{xy}) strain.*

We have also explored the topological phase diagram of monolayer and bilayer $ZrTe_5$ crystals under mechanical deformations, using *ab initio* calculations. The band structure of mono- and bilayers of $ZrTe_5$ is plotted in Fig. 1b, showing a 70 meV topological gap for the monolayer. In the bulk, changes to the interlayer spacing are a key parameter in shaping the topology of the band structure. This is reflected in the topological phase diagrams shown in Fig. 1, where the gap closes for modest strain in the van der Waals interlayer separation. As a function of in-plane biaxial deformation, the bilayer shows a transition from a trivial insulator to a topological insulator at experimentally achievable strains of a few %. At the same time, in the monolayer case there is no trivial-topological phase transition, only a closure of the topological gap for small (<1%) compressive strain. Thus, from a perspective of tuning topological phases via strain, bilayers of $ZrTe_5$ represent a unique platform realizing the topological-trivial insulator transition.

Since the preparation of monolayers and bilayers is still a challenge, we have also examined the exfoliation of $ZrTe_5$ onto gold substrates (Fig. 11). We found that this method is not suitable, as opposed to other 2D tellurides, due to strong attraction of the first layer to gold which destroys its crystalline structure. Thus, in future experiments it is worth exploring the

exfoliation of $ZrTe_5$ onto other clean metal surfaces, where the strong adhesion to the metal does not compromise the crystal structure of the material.

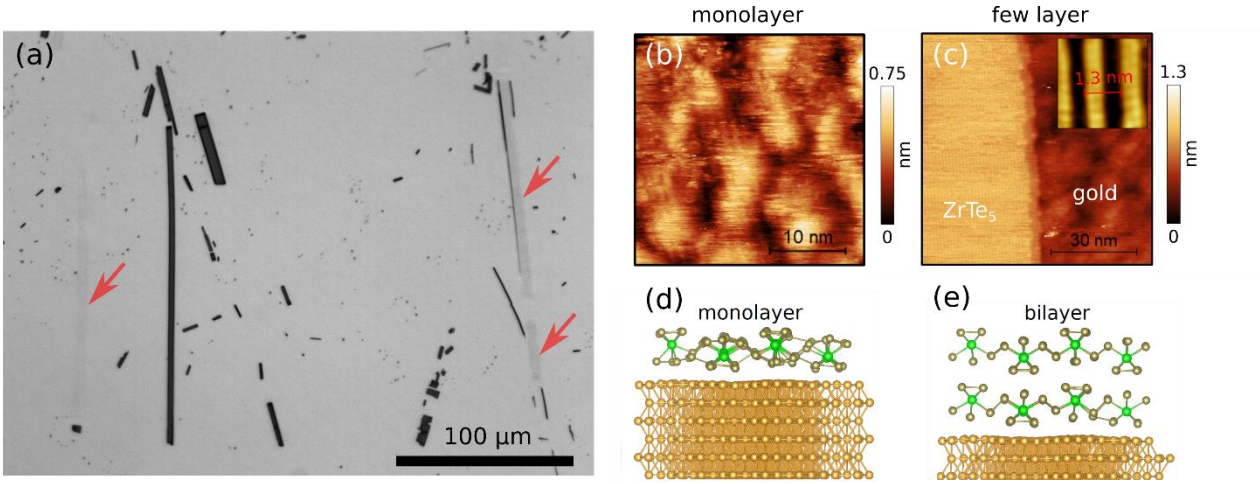

Fig. 11. *(a) Optical microscopy image of exfoliated $ZrTe_5$ on a gold substrate. Red arrows mark areas with the smallest optical contrast, possibly monolayers. (b) Representative STM topographic image of a low contrast area, showing a disordered structure. With only slight hints of unit cell periodicity. (c) STM topographic image of a few-layer area, showing a well resolved atomic contrast on top of the crystal. (d) Relaxed ab-initio model of an adsorbed $ZrTe_5$ layer on a gold (111) surface. (e) Calculation for a bilayer $ZrTe_5$. The crystalline structure of the monolayer is destroyed by the strong adhesion to the gold substrate, while in the bilayer case the top monolayer is unaffected.*

Strain-engineering the electronic and optical properties of graphene

Graphene plasmons are hybrids of Dirac fermions and photons, which are particularly appealing, due to their unmatched mode volume confinement, long lifetime and easy tunability. To fully exploit these unique properties, visible-frequency graphene plasmons are desirable, given that our most efficient optical techniques are available for visible light. However, tuning up the resonance frequency from native THz values into the visible range turned out particularly challenging. The most straightforward strategy to tune up the resonance frquency is the lateral confinement of plasmons into graphene nanostructures. It has been proposed that graphene structures below 10 nm characteristic size, can scale up plasmon frequencies into the visible. However, this approach is strongly limited by the detrimental effects of edges on plasmon resonances. We have demonstrated the realization of visible graphene plasmons through their edge-free lateral confinement into sub-5 nm graphene nanocorrugations with particularly high aspect ratios. Such graphene sheets with strong nanoscale corrugations were prepared by cyclic thermal annealing between room temperature and 400º C. Fig. 15 shows the topography obtained from Scanning Tunneling Microscopy (STM) investigations, revealing a graphene sheet with strong nanoscale corrugation. The RMS value characterizing the surface roughness is about 0.5 nm, which is almost the double of the RMS value measured in graphene on SiO_2 (0.27 - 0.35 nm). Graphene corrugations with aspect ratios (h_{max}/R) as high as 0.5 could be easily found. These numbers clearly highlight the extreme nature of the nanoscale deformation (corrugation) of our nanocorrugated graphene sheets

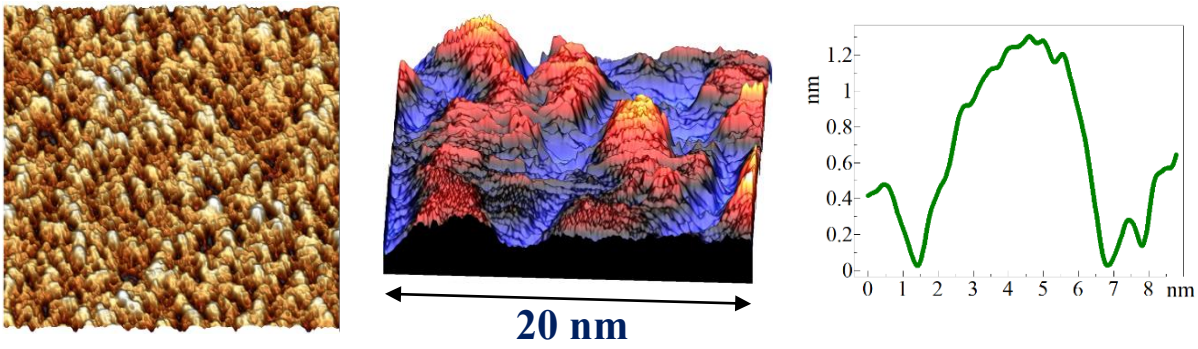

Fig. 15 *STM images of graphene sheets prepared by cyclic thermal annealing, displaying a particularly strong nanoscale corrugation, with lateral size below 10 nm, and nanometer height. Line cut displaying a typical graphene nanocorrugation geometry with an aspect ratio of* $h_{max}/R \sim 0.5$.

The most striking findings were observed when measuring the Raman spectra of nanocorrugated graphene sheets with 633 nm excitation wavelength. Such measurements revealed a huge Raman signal, only by exposing the samples to air (Fig. 16b). Detecting Raman peaks with 20 times higher intensity than the G peak of graphene by only air exposure is truly remarkable, and indicates a strong and robust underlying phenomenon. The huge Raman signal picked up form air, was identified as the fingerprint of copper phthalocyanine (CuPc) molecules. By atomic resolution STM images, we assured that the density of CuPc molecules on the surface of nanocorrugated graphene is very low (way below monolayer coverage). Consequently, the observation of Raman peaks that are twenty times higher than the graphene G peak must originate from a strong enhancement mechanism, rather than the large quantity of adsorbed molecules. As expected, exposing quasi-flat graphene sheets to the same conditions (i.e. air) does not result in any detectable CuPc signal in the Raman spectra (Fig. 16a).

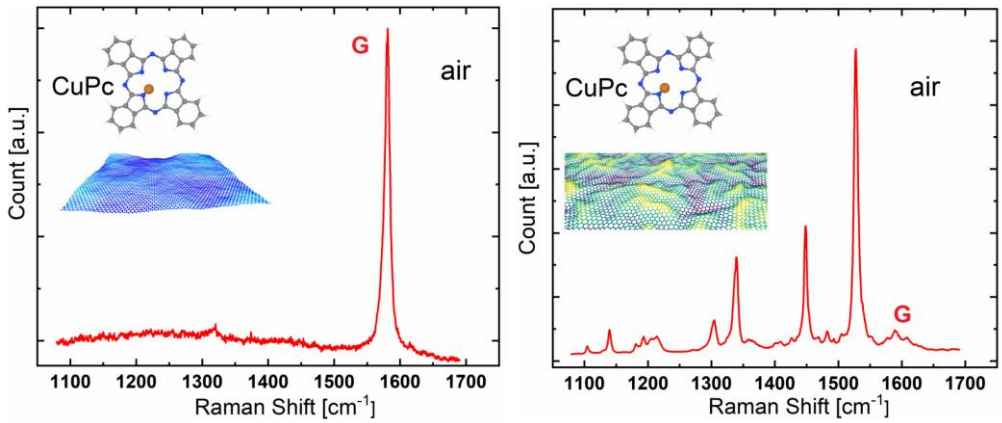

Fig.16 *Huge Raman enhancement on nanocorrugated graphene sheets. Detection of CuPc molecules form "clean" air by nanocorrugated graphene sheets (a). The Raman spectrum of quasi-flat graphene subjected to the same conditions is shown for reference (left).*

To gain insight into the origin of the increased optical response, we have calculated the electron energy loss spectrum of nanocorrugated graphene that directly reveals plasmon peaks. As apparent in Fig.17 several peaks appear in the calculated EELS spectra that can be associated with plasmons or quasi-plasmons of energies in the visible range.

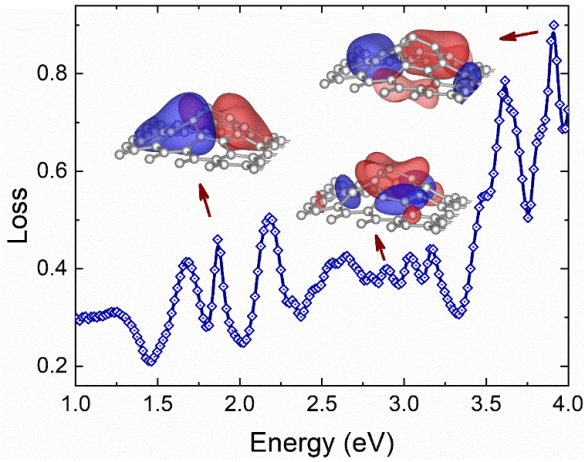

Fig. 17 *Calculated EELS spectrum of a model graphene nanocorrugation, revealing several loss peaks in the visible range. The insets display the charge distributions of optical excitations corresponding to different loss peaks.*

We have demonstrated the realization of visible graphene plasmons through their edge-free lateral confinement into sub-5 nm graphene nanocorrugations. The emerging strong near-fields of localized visible graphene plasmons provide such exceptional Raman enhancements that enable the detection of specific molecules even from air. This enormously enhanced interaction of molecules adsorbed on nanocorrugated graphene with visible light opens the way towards highly efficient and tunable SERS substrates and quantum emitters.

In summary, within this project we were able to achieve several important results, some of them according to the original plan, and some of them not foreseen at the moment of writing the proposal. Without doubt, the most important result is the realization of Pt nanoclusters with a novel atomic (bilayer) and electronic (energy gap of 0.3 eV) structure, characterized by a record intrinsic activity (turnover frequency). Such results emerged from the originally planned single Pt (heteroatom) modification of 2D MoS_2 crystals. Most importantly, the results we obtained from a slightly different outcome, actually exceed our original expectations regarding the improvement of catalytic activity of 2D MoS_2 crystals by heteroatom decoration. Even though the original idea of individual metal heteroatom modification of 2D crystals turned out way more challenging than expected, we were still able to achieve it taking a completely new approach with the help of our chemist colleagues. However, this last step has only been achieved during the fourth year of the project. Due to this, we are lagging behind with publications. At the moment there are four papers that present the results of this project under various stages of publications. From Pt-MoS_2 results a revised manuscript is prepared for Nature Energy that required a series of additional experiments. A manuscript is under preparation from the 2D Au clusters stabilized on 2D MoS_2, and their enhanced activity for hydrogen evolution. Regarding the single Fe atom modification of 2D MoS_2 crystals for enhanced catalytic activity, two manuscripts are under preparation. The first one, describing the synthesis and properties of a suitable Fe complex is under review in Dalton Transactions (a revived manuscript is prepared), while the manuscript reporting 2D MoS_2 crystals modified by single Fe atoms for enhancing its catalytic properties, is under preparation, and will be submitted in the next few weeks.